Effect of cholesterol on the rigidity of saturated and unsaturated membranes: fluctuation and electrodeformation analysis of giant vesicles†

Rubèn Serral Gracià,‡§ Natalya Bezlyepkina,§ Roland L. Knorr, Reinhard Lipowsky and Rumiana Dimova*

Received 2nd October 2009, Accepted 13th January 2010
First published as an Advance Article on the web 8th February 2010
DOI: 10.1039/b920629a

Two different methods for measuring the bending stiffness of lipid membranes are used and further developed: fluctuation analysis and vesicle electrodeformation. For this purpose, fast camera imaging was employed minimizing the experimental effort. The methods were applied to study the effect of cholesterol on the bending stiffness of two types of membranes. We explored giant vesicles prepared from dioleoylphosphatidylcholine–cholesterol and sphingomyelin–cholesterol mixtures. The results show that the effect of cholesterol on the bending stiffness is quite different and lipid-specific. While the bending stiffness of dioleoylphosphatidylcholine membranes does not change significantly, sphingomyelin membranes become more flexible with the addition of cholesterol. Finally, we report data on vesicles prepared from lipid extracts of the plasma membrane of human red blood cells and investigate the influence of naturally present transmembrane peptides. The latter molecules do not alter the membrane stiffness significantly.

Introduction

In order to understand the complex behaviour of lipid membranes, one has to elucidate their basic mechanical properties.[1] The significant expansion in recent years of the field of membrane raft-like domain formation[2,3] imposes the compelling need for data on the bending rigidity of membranes with different compositions, not only single-component but also binary, ternary and more complex mixtures. Furthermore, temperature and the presence of solutes in the membrane environment can influence the bilayer bending rigidity and, thus, lead to a variety of interesting membrane processes.[4,5] Therefore, it is essential to improve and develop methods for measuring the elastic properties of bilayers, which are easy to apply and do not require very extensive experimental effort and/or high-end equipment.

A large number of techniques to measure the bending rigidity of membranes has been applied previously, see the overview in ref. 6. The most popular method seems to be fluctuation analysis, which was established more than 30 years ago by Brochard and Lennon on erythrocytes[7] and Servuss *et al.* on tubular vesicles,[8] and later extended to giant vesicles.[9–14] This method is probably the least demanding from an experimental point of view, because it is based on the direct video microscopy observation of giant vesicles. Another method, less employed in the literature, is based on measuring the vesicle deformation induced by electric fields as introduced by Helfrich and co-workers.[15,16]

Max Planck Institute of Colloids and Interfaces, Science Park Golm, 14424 Potsdam, Germany. E-mail: Rumiana.Dimova@mpikg.mpg.de; Fax: +49 331 567 9612; Tel: +49 331 567 9615

† Electronic supplementary information (ESI) available: Lipid extraction from red blood cells, contour recognition and dye exclusion from solid domains. See DOI: 10.1039/b920629a

‡ *Present address*: Culgi B.V. P.O. Box 252 2300 AG Leiden, The Netherlands.

§ RSG and NB contributed equally to this work.

Here, we discuss these two methods, which as we will demonstrate, still offer room for improvement, whether from the aspect of experimental implementation (as in this work) or analysis involving the influence of factors like membrane-embedded proteins,[17,18] coupling to the cytoskeleton,[19] presence of charged lipids *etc.* In the following sections we outline problems and difficulties faced when using these two techniques, and offer possible solutions.

Using the two methods, we examine the effect of cholesterol on the bending stiffness of various types of membranes. Our measurements support a recently reported trend in the behaviour of membranes composed of unsaturated lipids and cholesterol.[20,21] In particular, data obtained from the two methods confirm that the addition of cholesterol to lipids with two mono-unsaturated chains like dioleoylphosphatidylcholine does not alter the bending stiffness of the membrane for a wide range of cholesterol compositions.

Furthermore, we report novel observations on the properties of vesicles composed of sphingomyelin and cholesterol. Our measurements cover a range of molar fractions of these two components, extending from the two-phase coexistence range to the liquid ordered phase. The latter is accompanied with a decrease in the effective bending stiffness of the membrane. To the best of our knowledge, this is the first systematic study about the effect of cholesterol on the bending stiffness of sphingomyelin membranes.

Apart from two-component bilayers, we apply the two experimental methods to more biologically relevant membranes composed of lipid extracts from the plasma membrane of red blood cells, which contain up to about 50 mol% cholesterol. We compare the bending stiffness of these membranes with the results obtained for sphingomyelin–cholesterol and dioleoylphosphatidylcholine–cholesterol membranes, as well as for membranes prepared from plasma membrane extract with transmembrane peptides.

The paper is organized as follows. After a description of the experimental procedures, the two methods—fluctuation analysis and vesicle electrodeformation—are discussed in detail. The results section is followed by a discussion of the effect of cholesterol on the bending stiffness of various types of membranes, and a brief conclusion.

Materials and methods

In the following subsections, we provide details about our protocols for vesicle preparation and observation. We emphasize the importance of osmotic stabilization of the vesicles and discuss possible effects of gravity on their shape fluctuations. Then, we introduce the experimental settings applied in the two methods for measuring the bending stiffness—fluctuation analysis and electrodeformation.

Vesicle preparation

The vesicles were prepared from dioleoylphosphatidylcholine (DOPC) and egg sphingomyelin (SM) from Avanti Polar Lipids Inc. (Alabaster, AL) and cholesterol (Chol) from Sigma (Steinheim, Germany). The explored membrane compositions were pure lipid and DOPC, SM and Chol binary and ternary mixtures, where the Chol fraction was varied between 0 and 50 mol%. Occasionally, we labelled the vesicles with 0.1 mol% 1,1′-dioctadecyl-3,3,3′,3′-tetramethylindocarbocyanine perchlorate (diIC18) from Molecular Probes (Leiden, the Netherlands) or 0.3 mol% perylene from Sigma. The fluorescent labelling did not lead to different values for the measured bending stiffness as compared to label-free membranes.

In addition to the lipids mentioned above, we also prepared vesicles from lipid extracts (LEs) from the plasma membrane of human red blood cells. The lipid extraction was performed according to the protocol of Bligh and Dyer,[22] for details see ref. 23 and the ESI†. The LE obtained in this way is known to contain about 10% phosphatidylserines, 14% phosphatidylcholines, 14% phosphatidylethanolamines, 11% sphingomyelines, and 50% cholesterol.[24]

We also investigated LE membranes containing transmembrane peptides. These membranes were obtained from purified red blood cell ghosts shaved by proteolytic digestion to remove protein loops and domains extending beyond the membrane bilayer surface. These proteoliposomes were used to grow giant vesicles, for details see the ESI†.

Giant unilamellar vesicles (GUVs) were prepared using the electroformation method.[25] A small amount (25 μl) of 4 mM lipid solution in chloroform was spread on the surfaces of two conductive glasses coated with indium tin oxide. The latter were kept under vacuum at 63 °C in a vacuum drying oven (Heraeus Vacutherm VT 6025, Thermo Electron GmbH, Langenselbold, Germany) for at least 2 h to remove all traces of the organic solvent. The two glasses separated by a 2 mm thick Teflon frame were assembled to form a chamber sealed with silicone grease (Baysilone-Paste, Bayer, Germany). The chamber was filled with preheated 0.01 M glucose solution. The glass plates were connected to the AC field function generator Agilent 33220A (Agilent Technologies Deutschland GmbH, Böblingen, Germany), and an alternating current of 1.1 V and 10 Hz was applied for 1 h and afterwards changed to 1.5 V and 5 Hz for another 2–3 h. The vesicles were grown at 63 °C to ensure that the lipids are in the fluid state and fully miscible. Tense spherical vesicles with sizes ranging from 10 to 100 μm were observed to form. In some sample preparations, the obtained vesicle suspension was subsequently diluted with glucose solution of slightly higher osmolarity. The solution osmolarities were adjusted with the cryoscopic osmometer Osmomat 030 (Gonotec, Berlin, Germany). In other sample preparations, the vesicle suspension was diluted with the glucose solution used for vesicle preparation and the observation chamber was kept loosely closed for several hours at room temperature. The evaporation of water, controlled by measuring the weight of the chamber with a balance, led to an increase in the outside solution osmolarity. In both cases, the achieved osmotic difference, which was on the order of 1–2 mOsm, was sufficient to deflate the vesicles, which were then characterized by very low membrane tension, as indicated by visible membrane fluctuations. Note that the osmolarity change achieved by dilution with hypertonic solutions is less suitable because it may lead to vesicle rupture or budding. In a few cases, a small amount of NaCl (leading to the final concentration of 0.1 mM) was added to the glucose solution used for dilution. The presence of salt did not lead to any significant changes of our results.

Growing the vesicles in glucose solution ensures osmotic stabilization, which keeps the vesicle volume constant throughout the measurements. Note that such stabilization is not achieved when the vesicles are grown in pure water. Using vesicles in pure water solutions should be avoided in methods where the vesicles are subject to external pressure as in the case of electrodeformation or micropipette manipulation, because the vesicle volume may change during the measurement. When vesicles are grown in sucrose and subsequently diluted in glucose, the density difference of the solutions leads to sedimentation of the vesicles to the chamber bottom. This trick has often been used in studies of giant vesicles. The associated gravity effects such as change in the shape of vesicles resting at the bottom of the chamber were either neglected in the fluctuation analysis, minimized by focusing on a certain subset of vesicles,[26] or taken into account by explicit shape calculations.[14] In this study, gravity effects influencing the vesicle shape were avoided because of the glucose symmetry across the membrane. In addition, possible effects arising from membrane adhesion to the glass surface were prevented.

Optical microscopy

An inverted microscope Axiovert 135 (Zeiss, Germany) equipped with 20× and 40× objectives was used to visualize the GUVs under phase contrast mode. Image sequences were recorded with a fast digital camera HG-100K (Redlake Inc., San Diego, CA). For routine observations, vesicle selection and electrodeformation measurements, the samples were illuminated with a halogen lamp. A mercury lamp HBO W/2 was used only for a short time of up to approximately 2 min to acquire images of fluctuating vesicles using the fast digital camera. All experiments were performed at room temperature (23 ± 0.5 °C). Sample heating due to illumination was measured using a fibre optic conditioner FTI-10 (FISO Technologies Inc., Québec, Canada)

immersed in the sample. The change in the temperature was less than 1 °C after 10 min of illumination, thus not significantly changing the bilayer properties during the measurements.

The observation chamber (Eppendorf, Hamburg, Germany) used for electrodeformation recordings and for comparative fluctuation analysis measurements consists of a Teflon frame confined from above and below by two glass plates. A pair of parallel cylindrical electrodes with a radius of 92 μm and a separation of 0.5 mm is fixed to the lower glass. The chamber was connected to an AC field generator. Additional fluctuation spectroscopy measurements were performed in a separate chamber made of two microscope slides separated by a 1 mm deep press-to-seal silicone isolator (Molecular Probes, Eugene, OR). The fluctuation analysis measurements on LE vesicles were mainly done in the latter chamber.

In the experiments, one often encounters vesicles with "defects" that may represent lipid lumps or membrane tubes (also called tethers) connected to the vesicle membranes. The membranes associated with these defects are highly curved. High curvature can lead to lipid sorting[27,28] and, thus, may induce composition gradients in the vesicle membrane. Therefore, we did not include such vesicles with "defects" in our analysis. Furthermore, we also excluded vesicles adhering to surfaces or other vesicles from our analysis since adhesion can induce domain formation and phase separation within the contact area.[29,30]

Typically, we selected a quasi-spherical vesicle with a mean radius between 15 and 40 μm. In most of the cases, the vesicles were first subjected to electrodeformation and their shapes then recorded for fluctuation analysis. In this way, the results obtained from the two techniques could be compared for the same vesicle.

Two techniques for measuring bending rigidity

Fluctuation or flicker spectroscopy. The analysis of shape fluctuations of membranes and vesicles is based on time sequences of snapshots as obtained by optical microscopy.

Two important time scales have to be considered for the image acquisition. The first one is the exposure time, also referred to as shutter speed, which is the time the camera shutter is open for image integration. On the one hand, the exposure time should be shorter than about 1 ms, otherwise all fast moving high-wavenumber modes are averaged out by the camera and therefore lost. For instance, for a typical vesicle with radius 10 μm and bending stiffness 10^{-19} J, and viscosity of the media 10^{-3} Pa s, the relaxation time of the mode with wavenumber 50 (corresponding to $n = 50$ in eqn (7)) is around 300 μs.[12,31] On the other hand, the exposure time may be longer than 10 μs because the optical resolution does not allow resolving small-wavelength deformations corresponding to modes with high wavenumbers and shorter characteristic times. Typical exposure times of conventional video cameras lie in the range 1–40 ms. In the past, this problem has been circumvented by removing the theoretically predicted effects of camera integration from the observed modes.[12] Here, we used a fast digital camera, which overcomes the above problems completely as it allows setting the exposure time down to 5 μs. In practice, the exposure times were selected in the range 70–200 μs.

The second important time is the acquisition time. To analyze the state of the system, a sequence of snapshots at different times is collected. This sequence must lead to a representative ensemble of shapes of the vesicle. In particular, the vesicle should be able to move through most of its available configurations, *i.e.*, it must span its phase space. This is especially crucial for the modes with low wavenumbers, which are very slow and need a few seconds to relax. We performed measurements with an acquisition of 1 min, which for vesicles with radius of the order of ten microns should be sufficiently longer than either the recurrence or the relaxation times of the excitation.[32] The acquisition speed was varied between 60 and 250 frames per second (fps), which leads to several thousand images per measurement.

The fast digital camera that we used did not allow direct video streaming onto the computer. Instead, the images are stored in the on-board memory of the camera head (total of 4 GB), and afterwards are downloaded to the computer. The images are analyzed to extract the vesicle contours (see the ESI†), followed by analysis of the fluctuations as explained below. The total procedure including measurement and analysis is completed within about 20 min.

As previously shown,[31] the position of the vesicle membrane can be described as

$$r(\theta,\phi) = R\left(1 + \sum_{lm} u_{lm} Y_{lm}(\theta,\phi)\right) \tag{1}$$

for shapes close to a sphere, where θ and ϕ are the polar and azimuthal angles, R is the averaged radius and u_{lm} are the weights of each of the spherical harmonics Y_{lm}. For a quasi-spherical vesicle, the dimensionless mean square amplitudes of the spherical harmonic modes behave as

$$\left\langle \left|u_{lm}\right|^2 \right\rangle = \frac{k_B T}{\kappa(l+2)(l-1)[l(l+1)+\bar{\sigma}]} \tag{2}$$

Here $k_B T$ is the thermal energy and $\bar{\sigma} = \sigma_{\mathrm{eff}} R^2/\kappa$ introduces the effective tension σ_{eff}, where κ is the bending stiffness of the membrane. Note that σ_{eff} can attain negative values, *e.g.* for very deflated quasi-spherical vesicles.[33,34]

In the experiment, we can obtain information solely from the focal plane. Eqn (2) depends only on l and not m, allowing us to study the fluctuations of the vesicle by observing just one plane, not requiring a three dimensional measurement. Since the sharpest image corresponds to the equatorial plane of a vesicle, we use only the information from the focal plane by setting the polar angle to $\theta = \pi/2$. The two-dimensional contours are[32]

$$v(\phi) \equiv v(\pi/2,\phi) = R\sum_{q=0}^{q_{\max}} v_q e^{iq\phi} \tag{3}$$

Comparing eqn (3) and (1) for $\theta = \pi/2$ one finds the following expression for the mean square amplitudes in the equatorial plane (which here coincides with the focal plane because gravity has no effect on the vesicle shape):

$$\left\langle \left|v_q\right|^2 \right\rangle = \sum_{l=q}^{l_{\max}} \left\langle \left|u_{lq}\right|^2 \right\rangle P_{lq}(\cos\ \pi/2) N_{lq} \tag{4}$$

Here $l_{\max}$ is the cut-off of the shortest possible wavelength, P_{lq} is the Legendre polynomial from the spherical harmonics, and $N_{lq} \equiv [(2l+1)/4\pi][(l-q)!/(l+q)!]$ is a normalization factor.

One can extract the bending rigidity from this expression as

$$\kappa/k_BT = S(q) \Big/ \left\langle |v_q|^2 \right\rangle \tag{5}$$

where

$$S(q) = \sum_{l=q}^{l_{\max}} \frac{N_{lq}\left[P_{pq}(\cos\ \pi/2)\right]^2}{(l+2)(l-1)[l(l+1)+\bar{\sigma}]} \tag{6}$$

$l_{\max}$ is estimated to be around 10^4, however, for moderate tension σ_{eff} (or $\bar{\sigma}$), eqn (6) converges rapidly, making it sufficient to consider a few hundred terms in the sum.

After obtaining the vesicle contours (see the ESI†), we perform the following analysis. Each point of the contour, r_i, is rescaled by the averaged radius R, *i.e.*, the zeroth Fourier mode. The modes of the Fourier-expanded contour are defined as follows:[26]

$$a_n = \frac{1}{2\pi}\sum_i \Big\{ r_i \cos(n\theta_i) + r_{i+1}\cos(n\theta_{i+1}) \Big\}(\theta_{i+1} - \theta_i) \tag{7a}$$

$$b_n = \frac{1}{2\pi}\sum_i \Big\{ r_i \sin(n\theta_i) + r_{i+1}\sin(n\theta_{i+1}) \Big\}(\theta_{i+1} - \theta_i) \tag{7b}$$

Taking the variance of these coefficients we obtain

$$\left\langle |v_q|^2 \right\rangle = \frac{1}{4}\left[\left\langle \left[a_q(t_i) - \langle a_q \rangle\right]^2 \right\rangle + \left\langle \left[b_q(t_i) - \langle b_q \rangle\right]^2 \right\rangle \right] \tag{8}$$

where the time dependence has been made explicit and $\langle x \rangle = (1/N)\Sigma_i^N x(t_i)$ stands for the average of all the contours. The measured $\langle |v_q|^2 \rangle$ can be now introduced in eqn (4) and one can obtain κ and σ_{eff} by means of a fit. To perform this fit, the sum in eqn (6) has to be recomputed for each try of σ_{eff}. The algorithm performs well since the prefactor needs to be computed only once.

There are three regimes in the behaviour of the experimentally measured variance. As seen from eqn (2), for the low-wavenumber modes, the tension σ_{eff} dominates the fluctuations. In addition, the statistics is poor for these modes, which is why they are typically ignored in the analysis. For intermediate modes, the variance scales as the inverse cube of the wavenumber, q^{-3}. This is the regime used to obtain the bending rigidity modulus. For high-wavenumber modes, the data are dominated by noise and can no longer be analyzed.

Sometimes, for tense vesicles or for bad quality contours, the q^{-3} behaviour cannot be distinguished. Vesicles that did not show a recognizable plateau for intermediate modes in a plot of reduced mean square amplitudes $\langle |v_q|^2 \rangle\, q^3$ as a function of q were excluded.

Vesicle electrodeformation. During electrodeformation, a selected vesicle is subjected to an AC electric field of increasing strength and the induced shape deformation is recorded.[15,16] Vesicle electropermeabilization is not observed as we conclude from the microscopy images and the preserved vesicle volume. At relatively low field frequencies around 2 kHz, formation of large pores of several micrometres in giant vesicles may occur, as previously reported.[35] Thus, in our experiments, higher frequencies in the range between 25 kHz and 300 kHz have been chosen. In a couple of cases we also explored frequencies down to 1 kHz, but electroporation was not observed. For the conductivity conditions used here, the vesicles assume prolate deformation in the explored frequency region.[36–38]

For the electrodeformation analysis study, the camera exposure time is not relevant since we are only interested in the maximal elliptical deformation adopted by the vesicle. However, the acquisition time after applying the field (or changing the field strength) should be long enough to assure that the vesicle deformation has attained a steady state. We applied the electric field using a stepwise increase of the field amplitude, typically by a step of 0.2 V. No hysteresis in the vesicle deformation was observed when decreasing the potential. This procedure was automated using a home-written program, which changes the applied potential of the wave function generator, and records and analyses the vesicle response. The acquisition rate was set to 30 fps. The vesicle contour was detected as described in the subsection "Fluctuation or flicker spectroscopy" and in the ESI†. One example of vesicle deformation arising from the stepwise increase in the field strength over time is shown in Fig. 1. The degree of deformation is expressed as the aspect ratio a/b, where a and b are the vesicle semi-axes along and perpendicular to the field direction, respectively, see inset in Fig. 1. Observations on the response time of different vesicles suggested that typically 2 s are sufficient to reach the steady state deformation after changing the potential of the field (shaded zones in Fig. 1). Images recorded in the following 3 to 8 s were used for averaging over the stationary shape in time to achieve better precision.

The vesicle deformation is associated with a change in the apparent area due to flattening of the membrane fluctuations. This behaviour has been described in the literature for flat bilayers[39] and quasi-spherical vesicles.[31] Area stored in the high-wavenumber modes is pulled to give rise to deformations described by the second mode, corresponding to $n = 2$ in eqn (7), and thus, made visible. The area change is expressed as[39,40]

$$\alpha \equiv \frac{A - A_0}{A_0} = \frac{k_BT}{8\pi\kappa}\log\left(\frac{\sigma}{\sigma_0}\right) \tag{9}$$

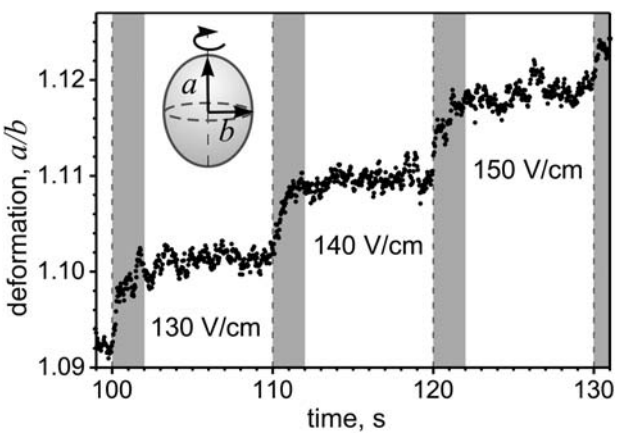

Fig. 1 Degree of deformation, a/b (as indicated in the inset) induced on a vesicle made of DOPC : Chol 9 : 1 with radius of 66 μm, subjected to the AC field. The field frequency was 200 kHz. The applied electrical potential was increased every 10 s with a step of 0.5 V (1 kV m^{-1}), as indicated. The first 2 s after changing the field (shaded zones) were excluded from averaging over the shape in time.

where A is the area of the ellipsoid, A_0 is the area of the sphere with the same volume, and σ_0 is the positive parameter obtained by extrapolation to $\alpha = 0$. Note that σ_0 can be larger than the actual tension at zero field strength. Indeed, obtaining the exact value of this parameter is not necessary for evaluating the bending rigidity of the membrane. In our image analysis, the area change was estimated from the second mode of the vesicle deformation expanded in Legendre polynomials.[41] The tension of the deformed vesicle, σ, can be obtained from the electric stresses. Since the pressure inside the vesicle must be constant, combining the Laplace equation at the poles and the equator gives

$$(c_1 + c_2)_{equ}\sigma - (T_{rr})_{equ} = (c_1 + c_2)_{pol}\sigma - (T_{rr})_{pol} \quad (10)$$

where c_1, c_2 are the principal curvatures taken either at the equator (equ) or the pole (pol), and therefore measurable from the geometry of the vesicle. The normal electric stresses at the equator and the poles of the vesicle[15,16]

$$(T_{rr})_{equ} - (T_{rr})_{pol} = g\varepsilon_w E_0^2 \quad (11)$$

where ε_w is the dielectric constant of water, E_0 is the field strength far away from the vesicle and g is a dimensionless parameter which is a function of the field frequency, the dielectric constants of the membrane and the solutions inside and outside the vesicle. For a given frequency, g is a constant that cancels out if one considers the ratio σ/σ_0 (as obtained from eqn (10) and (11)) needed to estimate the membrane bending rigidity following eqn (9). The curvatures in eqn (10) can be obtained from the amplitude of the second mode in the Legendre polynomial expansion. This approximation is valid for elliptical vesicles and small deformation. For high field strength (the maximum applied field strength was 20 kV m^{-1}), the vesicle shape may start to deviate from ellipse, *e.g.*, attaining pointier poles. Thus, it is more appropriate to take into account higher modes (in this work, we have implemented analysis including the fourth mode in the Legendre polynomial expansion).

Logarithmic plot of the rescaled lateral tension, σ/σ_0, obtained from eqn (10) against the change in apparent area gives a straight line with slope related to the bending rigidity as described by eqn (9). Note that for very low field strength, the vesicle deformation may be small and the change in the second mode becomes comparable to the noise (see *e.g.* Fig. 3). For such cases, data points in this voltage region were ignored.

Note that this method does not apply to vesicles containing charged lipids (which is the case of LE vesicles) and in salt solutions. In these cases, the Maxwell stress tensor used to evaluate the membrane tension induced by the electric field has to account for the media conductivity and the excess charge at the membrane surface (T. Yamamoto, S. Aranda, R. Dimova and R. Lipowsky, unpublished).

Results

To directly compare the results for the membrane bending stiffness obtained from the two methods, fluctuation analysis and electrodeformation, we first present data from both techniques applied to the same vesicle. The considered example is a vesicle composed of DOPC : Chol 9 : 1 with a radius of 26.5 μm.

For fluctuation analysis, the vesicle images were recorded for over 1 min, exposure time of 200 μs and with acquisition rate of 60 fps, yielding 3745 contours. Evaluation of the mean square amplitudes by eqn (4)–(6) provides the q-dependence of the bending modulus κ of the vesicle as shown in Fig. 2. The three regimes discussed in the subsection Fluctuation or flicker spectroscopy are easy to distinguish. The tension-dominated regime observed for the low-wavenumber modes gives way to a plateau at intermediate modes where κ is practically independent of the wavenumber. At $q > 25$ the fluctuations are dominated by noise and are not considered in the analysis. The intermediate regime with $6 < q < 25$ is the one which provides us with the mean value of $\kappa = (14.23 \pm 0.45) \times 10^{-20}$ J. For the effective vesicle tension we obtain $\sigma_{eff} = (1.98 \pm 0.56) \times 10^{-9}$ N m^{-1}. Repeating the measurement on the same vesicle shows reproducibility of κ within about 17% deviation. The bending stiffness measured on different vesicles with the same composition shows scatter within about 20% of the absolute value of κ. The effective tension was found to vary between -5×10^{-9} N m^{-1} and 2×10^{-7} N m^{-1}. Note that the vesicle preparation protocol does not allow producing vesicles with specific tension. For the measurements, we have chosen vesicles, which visibly flicker under the microscope. For the tension range explored in our experiments no appreciable change in the intrinsic area per molecule is expected. Thus, the tension, which is vesicle-specific, does not have an effect on the membrane material properties like the bending rigidity.

The same vesicle was subjected to electrodeformation by an AC field with frequency 300 kHz and field strength increasing stepwise by 0.2 V, which taking into account the inter-electrode distance is equivalent to a field strength of 0.4 kV m^{-1}. The snapshots in Fig. 3a illustrate the field-induced vesicle elongation. The dependence of the relative area change as a function of the applied tension is given in Fig. 3b. A linear least squares fit following eqn (9) yields for the slope $\kappa = (9.0 \pm 0.4) \times 10^{-20}$ J. Repeating the measurement on the same vesicle shows

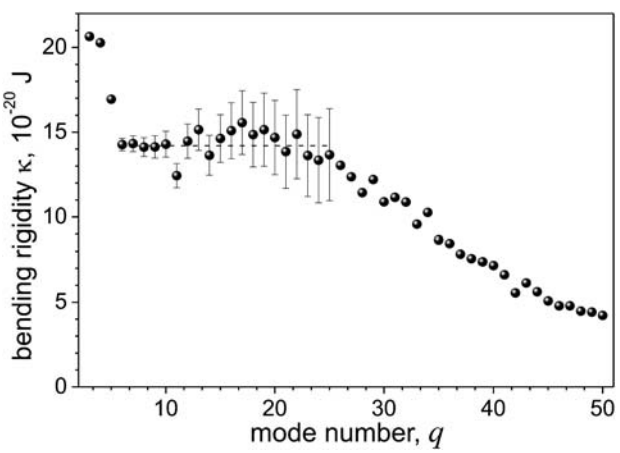

Fig. 2 Mode number dependence of the bending rigidity κ of a DOPC–Chol 9 : 1 vesicle with radius 26.5 μm. The error bars are given only for the intermediate regime used to estimate the mean value of κ. The dashed line corresponds to a fit in the range $6 < q < 25$.

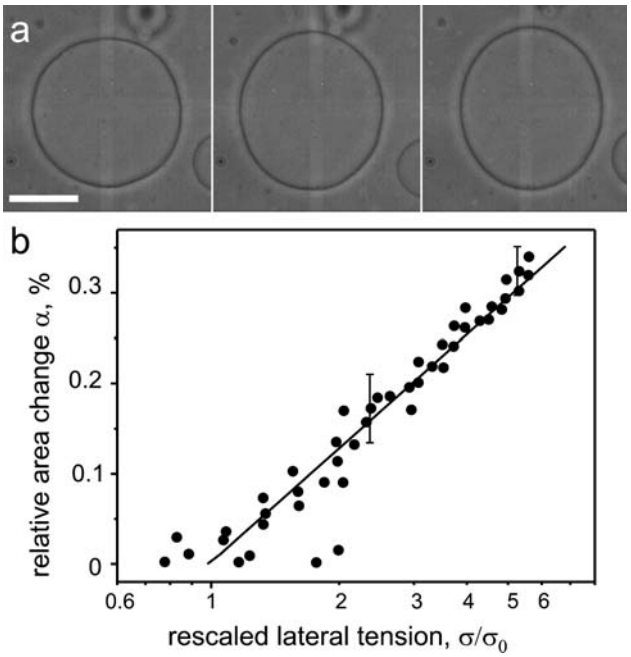

Fig. 3 Deformation of a vesicle subjected to an AC field at 300 kHz and variable strength. The same vesicle was analyzed in Fig. 2 by fluctuation spectroscopy. (a) Phase contrast images of the vesicle at field amplitudes 2, 10 and 20 kV m^{-1}. The scale bar corresponds to 25 μm. (b) Relative area change as a function of the normalized membrane tension. The field strength was increased in a stepwise manner with increment of 0.4 kV m^{-1}. Each data point is a result of averaging the relative area over 90 images. The solid line is a linear least squares fit, with a slope yielding $\kappa = (9.0 \pm 0.4) \times 10^{-20}$ J for the bending stiffness.

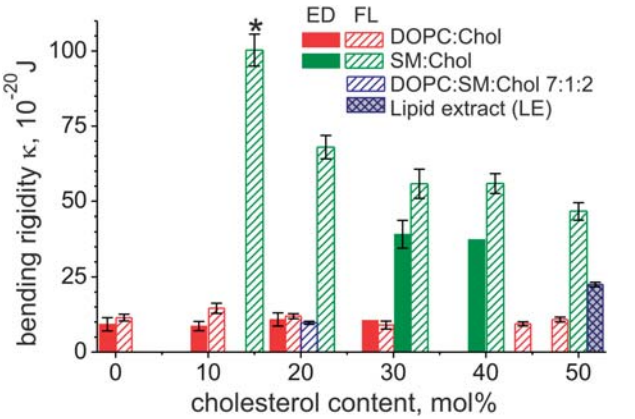

Fig. 4 Bending rigidity of membranes made of different lipids as measured (i) by the electrodeformation method, indicated in the legend as ED (solid bars), and (ii) by fluctuation spectroscopy, indicated as FL (hatched bars). The error bars show the standard error from the mean value of a population of vesicles. The absence of an error bar indicates a single measurement. The values for the bending rigidity of SM : Chol 85 : 15 indicated with a star (*) were measured on 5 specially selected vesicles: for all other vesicles in the sample, fluctuations were not observed, suggesting that these five vesicles were not representative ones. All measurements were performed at 23 °C.

reproducibility of the value within about 22% deviation. Scatter within about 25% of the obtained bending stiffness is observed when the measurements are performed on different vesicles with the same composition.

Within the accuracy of the two methods, the obtained values for the bending stiffness κ are in agreement. Using the two approaches, we explored membranes with the following lipid compositions: pure DOPC, DOPC : Chol with 90 : 10, 80 : 20, 70 : 30, 56 : 44 and 50 : 50 molar ratios, SM : Chol with 85 : 15, 70 : 30, 60 : 40 and 50 : 50 molar ratios. We also performed measurements on membranes composed of the ternary lipid mixture DOPC : SM : Chol at 70 : 10 : 20 molar ratio, which at room temperature is in the one-phase region.[42] In addition, vesicles made of LE containing approximately 50 mol% cholesterol, see section Vesicle preparation for the specific lipid composition, were also studied. Furthermore, LE vesicles with transmembrane peptides were also explored. Altogether, about 170 vesicles with different lipid compositions were measured, the majority of which have been subjected to both methods. Note that because LE vesicles contain charged lipids, the electrodeformation method was not applied to these vesicles and only data from fluctuation analysis are presented. The results for all lipid compositions obtained from the two methods are summarized in Fig. 4 and Table 1 as a function of cholesterol content.

We observed a weak tendency for the electrodeformation approach to give slightly lower values for the bending stiffness than those obtained from fluctuation analysis. This effect is insignificant for softer membranes but appreciable for the stiffer SM : Chol membranes, see Fig. 4. In previous studies, it has been already discussed that mechanical methods like electrodeformation and micropipette aspiration give generally lower values for κ.[15,44] In the following section we will consider possible reasons for the small discrepancy between our results as obtained from fluctuation spectroscopy and electrodeformation. Effects of silicone grease as reported in ref. 16 are to be excluded because, for the measurements performed in our observation chamber, the vesicles were not in contact with any sealing substance. In addition, fluctuation spectroscopy measurements performed in chambers sealed with silicone spacer did not show any difference. The data reported in ref. 16, both with and without silicone grease, lead to significantly lower values for κ than those obtained by other groups and in the present study, see Table 1.

Discussion

Factors influencing the bending rigidity as measured by different methods

At tensions in the higher limit of the range explored with the electrodeformation method, the contribution to the measured relative area change, α, may not be uniquely caused by pulling out membrane undulations, but also partially arise from stretching (note that eqn (9) is valid in the limit of small tensions). The error in assessing the real surface tension in micromechanical experiments and the associated artificial reduction in the measured bending stiffness with such methods has been theoretically treated in ref. 44. To estimate the latter discrepancy the following correction factor was proposed:

$$f \approx 1 - 8\pi\kappa\sigma/(k_B T K_a) \quad (12)$$

Table 1 Bending rigidity, κ, of membranes with various compositions as obtained in the present study and reported in the literature. Our measurements were performed at 23 °C. The error in κ represents the standard error from the mean value for a population of vesicles. The results for the bending rigidity of the mixture SM : Chol 85 : 15 from Fig. 4 were not included because they were collected on 5 vesicles, which we cannot consider as representative

Membrane composition	κ, 10^{-20} J (present study[a])	Literature values for k, 10^{-20} J
DOPC		
	10.8 ± 1.0 (18)	8.5 ± 1 at 18 °C[45]
		7.6 ± 0.5 at 30 °C[20]
		8.5 ± 0.1 at 15 °C[20]
		1.6 − 1.7 ± 0.5[b] at 21 °C and 2.4–6.1 ± 1.2[b] at 23 °C[16]
DOPC : Chol		
90 : 10	11.6 ± 1.3 (18)	8.0 ± 0.8 at 30 °C[21]; 6.9 at 30 °C[50]
80 : 20	11.3 ± 1.2 (11)	7.3 ± 0.8 at 30 °C[21]; 7.2 at 30 °C[50]
70 : 30	9.2 ± 1.3 (8)	7.4 ± 0.8 at 30 °C[21]
56 : 44	9.4 ± 0.7 (9)	
50 : 50	10.8 ± 0.8 (12)	12 ± 1.2 at 22 °C[49]
SM : Chol		
80 : 20	68.2 ± 4.2 (12)	
70 : 30	55.8 ± 4.9 (11)	
60 : 40	55.9 ± 3.3 (14)	
50 : 50	46.7 ± 2.8 (18)	31 ± 2[c] at 22 °C[49]
DOPC : SM : Chol		
70 : 10 : 20	9.7 ± 0.5 (18)	
30 : 50 : 20		19 ± 5[c,d]; 80 ± 10[c,e] at 20 °C[43]
Red blood cell membranes		
LE (~50%Chol)	22.5 ± 0.8 (13)	26.8–47[f] at 25 °C[51]
LE with transmembrane peptides (~40%Chol)	22.5 ± 1.3 (8)	
Sterol-free LE		10 ± 1.5[f] at 25 °C[51]

[a] The values in brackets indicate the number of measured vesicles per composition. [b] The values for κ reported in this reference were found to depend on the presence of silicone grease and on the applied method. [c] The reported value for κ is for brain SM. [d] The reported value is for the liquid disordered phase. [e] The reported value is for the liquid ordered phase. [f] The lipids in these measurements were from whole-cell extracts and not from plasma membrane extracts as used here. The cholesterol content in these membranes was 40 mol%.

Here K_a is the stretching elasticity modulus. The real bending stiffness modulus can be estimated from the experimentally measured one rescaling it with f. The correction depends on the tension range. Unfortunately, data for the stretching elasticity of SM : Chol membranes, which exhibit the largest discrepancy between the two methods, does not seem to be available. For pure DOPC at 21 °C, $K_a = 265 \pm 18$ mN m^{-1}.[45] For tensions in the range 10^{-6} N m^{-1} to 10^{-4} N m^{-1} and bending modulus 9.26×10^{-20} J as measured by the electrodeformation method, the correction yields from 0.2% to 27.2% resulting in a value of 11.78×10^{-20} J for the higher tension. The latter value corresponds very well to the value for the bending rigidity as deduced from the fluctuation analysis modulus and given by $\kappa = 11.47 \times 10^{-20}$ J. It is worth noting that the correction may be even higher for membranes such as SM : Chol with a larger bending rigidity.

Note that the correction discussed above is comparable to the measurement accuracy and the scatter of the data collected on vesicles with the same composition. Other potential factors influencing the value for the bending stiffness obtained by electrodeformation are related to the magnitude of the applied field. Below, we list some of them to be considered if other groups intend to use this method. We point out possible ways to tackle the associated difficulties, and estimate the corresponding error.

First, the presence of other vesicles in the solution may shield the field. To avoid this, we typically selected isolated vesicles in whose vicinity no other vesicles were visible within the field of view of the camera.

Second, the chamber geometry may lead to an inhomogeneous field distribution, which can cause inhomogeneous stress distribution in the membrane. Such a stress distribution was recently reported to induce lipid flow in vesicles resting close to the chamber bottom.[46] A possible solution would be to design a chamber with thicker electrodes and a larger gap between them. Here, we avoided this effect by working with "light" vesicles, which were characterized by low density difference between the enclosed and surrounding solutions, and thus were not resting at the chamber bottom.

Third, the location of a selected vesicle with respect to the two cylindrical electrodes may also be important for evaluating the amplitude of the field experienced by the vesicle. The field is enhanced in the vicinity of the electrodes. We used the commercially available modelling package COMSOL (Multiphysics, Germany) to obtain the field distribution in our chamber based on finite element calculation, see also ref. 46. For vesicles located closer than about 40 μm away from the electrode and between 15 and 90 μm above the chamber bottom, the field magnitude could vary by more than about 10% from the one for a homogeneous field between two planar and parallel electrodes. This correction can change the value of κ by about 5%. In general, we avoided working with vesicles located very close to the electrode. Indeed, vesicles experiencing inhomogeneous fields become slightly asymmetric. This is reflected in the average value of the third mode of the vesicle contour expansion, which attains some non-zero value. In this article, data from such vesicles were discarded.

Finally, in a limited set of experiments (data not shown), the vesicles exhibited dielectrophoretic motion, which can additionally influence the value obtained for κ.

The factors listed above explain the slightly larger error in the values for the bending rigidity as measured by the electrodeformation method compared to the fluctuation analysis. Nevertheless, given the accuracy of the measurements, the values for κ obtained by the two approaches are very similar. In addition, as we will discuss further, the results obtained on membranes with different composition correspond well to values reported previously, suggesting that the two approaches provide reliable data.

Effect of cholesterol content on the bending rigidity

The bending rigidities of all membranes studied here are summarized in Table 1. For comparison, we include values reported in the literature for membrane compositions measured previously with other methods. Apart from fluctuation analysis and electrodeformation, other techniques previously applied to measure the bending rigidity of membranes containing cholesterol are micropipette aspiration,[40,45,47] tether pulling,[48,49] and diffuse X-ray scattering from bilayer stacks,[20,21,50] see also the review of Marsh.[6]

Our results indicate that addition of cholesterol to DOPC membranes does not influence the bending stiffness, in agreement with recently reported data,[21] see Table 1. This behaviour contradicts the widely accepted view that cholesterol increases the membrane bending rigidity in general. The conventional belief is that above the lipid phase transition temperature, cholesterol orders the acyl chains, inherently leading to an increase in κ. This concept was supported by observations on lipids such as stearoyloleoylphosphatidylcholine (SOPC),[40,48] dimyristoylphosphatidylcholine (DMPC),[13,51] palmitoyloleoylphosphatidylcholine (POPC) (not only in mixtures with cholesterol but with other sterols as well).[52] However, as demonstrated recently[21] and in the present study, the bending rigidity of DOPC–cholesterol mixtures does not show any significant correlation with the cholesterol content. The previous reports from the group of Nagle[20,50] were based on measurements of the diffuse X-ray scattering from bilayer stacks. Here, we confirm this tendency with two other methods—fluctuation analysis and electrodeformation of vesicles. In addition, we extend the explored range of cholesterol fraction to 50 mol%.

A major difference between DOPC and the above-mentioned lipids is that each of the acyl chains of DOPC contains a double bond. The affinity of cholesterol to phosphocholine membranes was found to decrease markedly with the increase in the degree of unsaturation of the lipid chains.[53] The influence of the degree of saturation on the cholesterol-dependent bending rigidity of various lipid membranes was previously explored by Pan *et al.*[21] This study was performed on bilayer stacks, the properties of which are, in general, different from those of freely suspended single bilayers. Here, we used giant vesicles in which, contrary to bilayer stacks, the membrane is fully hydrated and its fluctuations are not constrained by neighboring membranes. The trend observed in ref. 21 on DOPC : Chol membranes is confirmed by our results, but data for κ of almost fully saturated lipids like SM mixed with cholesterol, *i.e.* membranes in the liquid ordered phase, were not provided. SM has only one double bond in one of the acyl chains, which is located close to the headgroup region. The trend in the bending stiffness exhibited by SM : Chol mixtures follows neither the behaviour of lipids with one mono-unsaturated chain such as SOPC, which are characterized by a bending rigidity that gradually increases with cholesterol content, nor the one of lipids with two mono-unsaturated chains such as DOPC, which exhibit bending rigidities that are hardly affected by the cholesterol content. Instead, the addition of cholesterol from 20 to 50% to SM membranes leads to a gradual decrease in the membrane bending stiffness by about 30%.

The SM vesicles containing 15% Chol are a special case. While some of the vesicles exhibited shape fluctuations, others appeared to be rather rigid. The measurements reported in Fig. 4 were collected on the subset of vesicles with visible shape fluctuations. This suggests that not all vesicles in the batch have identical composition and that this composition is located in the coexistence region of the solid and the liquid ordered phase. Budding and fission of one of the phases would lead to two vesicles, each of which is either in the liquid ordered or in the solid phase.

At room temperature, the temperature at which our measurements were performed, pure SM membranes are in the solid phase. The phase transition temperature of egg SM is 39 °C.[54] The natural extract egg SM used in this work is predominantly (84%) composed of palmitoyl sphingomyelin (PSM). It does not exhibit the broadening of the melting transition as observed for porcine brain SM and bovine milk SM,[54] which contain fractions of unsaturated lipids. Thus, it is reasonable to expect differences in the phase diagrams of SM : Chol mixtures depending on the type of SM used as discussed below.

At very low cholesterol concentrations (below about 8 mol%) the membrane remains in the solid state.[55–57] The addition of cholesterol prevents lipids from condensing into the solid phase, induces the formation of liquid ordered phase and in such a way makes the membrane more fluid. This behaviour is thus reflected in the mechanical properties of the membrane such as the bending rigidity. At high cholesterol fraction, the membrane is in the liquid ordered phase. In the intermediate region, solid and liquid ordered phases coexist. The boundaries of this coexistence region as reported in the literature depend on the type of the SM and/or the method used for resolving the phase diagram.[42,58] Differential scanning calorimetry measurements show that the addition of cholesterol (up to about 10 mol%) causes a slight decrease in the temperature of the transition peak of egg SM followed by a modest increase at higher cholesterol concentrations and decrease and abolishment of the transition cooperativity.[59] Let us emphasize that egg SM is a lipid mixture, thus the phase diagram should differ from that of PSM : Chol and the coexistence region may be shifted and have a different width. PSM membranes containing cholesterol in the range roughly between 10 and 30 mol% exhibit coexistence of solid and liquid ordered phases.[55] However, this was not observed with fluorescence microscopy on giant PSM : Chol vesicles.[42] Possible explanations for this discrepancy are that the solid domains were not distinguished because the used fluorescent probe partitions equally in the two phases or because the domains are smaller than 1 μm.

Here, we used the fluorescent probe perylene in an attempt to distinguish solid domains in the coexistence region of egg SM : Chol membranes. Note that this coexistence region does not necessarily correspond to that measured in PSM : Chol membranes because of the additional lipid components (16%) in

egg SM. Perylene is excluded from solid domains in giant vesicles composed of mixtures of DOPC, egg SM and cholesterol in the 3-phase coexistence region of solid, liquid ordered and liquid disordered phases (see the ESI†). Thus, we expected to detect dye exclusion in egg SM : Chol membranes as indicator that the membranes were in the coexistence region of solid and liquid ordered phases. Such dye exclusion was not observed for cholesterol fractions above 15%, suggesting that our membranes were either in the liquid ordered state, or that the solid domains were smaller than 1 μm. In both cases, the measured bending rigidity in the region of 20–50% Chol is an effective value mainly corresponding to the properties of the liquid ordered phase. Note that in vesicles with stiff inclusions, like transmembrane proteins or peptides as discussed further, the effective bending rigidity will also reflect the properties of the fluid lipid bilayer mainly.

Systematic data on the bending rigidity of SM : Chol membranes in the liquid ordered state are not available in the literature. The only measurement provided by tether pulling experiments[49] was performed on membranes composed of brain SM : Chol 1 : 1 yielding a value, which is slightly lower than our result, see Table 1. The affinity of cholesterol to egg and brain SM and PSM was found to be comparable,[60] but some difference in the bending stiffness is still to be expected because in contrast to egg SM, brain SM contains about 20% of unsaturated lipids rendering the membrane more fluid and flexible.

The bending stiffness of DOPC : SM : Chol membranes in the liquid ordered phase,[43] see Table 1, was reported to lie in the range of values for SM : Chol membranes as measured here suggesting consistence of the results.

When systematic data are not available, one can consider estimating the membrane bending stiffness from the stretching elasticity modulus, K_a according to the expression[61,62]

$$\kappa = K_a h^2/\gamma \tag{13}$$

where h is the membrane thickness and γ is a numerical constant. A polymer brush model supported by experimental measurements yields $\gamma = 24$,[45] but note that there h is not exactly the membrane thickness as defined here. In contrast, molecular dynamics simulations lead to $\gamma \cong 48$, in agreement with a simple model based on classical elasticity theory.[61]

The stretching elasticity modulus of brain SM : Chol 1 : 1 membranes was measured with micropipette aspiration at temperatures 15 and 35 °C.[63] Interpolation for 25 °C gives for K_a approximately 2800 mN m^{-1}. Applying eqn (13) for this case and assuming $h = 4$ nm and $\gamma = 48$, yields the very rough estimate $\kappa \cong 93 \times 10^{-20}$ J. This value is somewhat higher than the value reported on brain SM : Chol 1 : 1[49] and even the value we measure for egg SM : Chol 1 : 1 vesicles, see Table 1.

Since data on the behaviour of the stretching elasticity modulus of SM : Chol membranes as a function of cholesterol fraction are not available, we consider data on K_a for dipalmitoylphosphatidylcholine (DPPC) membranes with cholesterol, which are also in the liquid ordered phase.[64] The value of K_a of such membranes was observed to decrease with cholesterol content from 10% to 15% but then drastically increase—almost three fold—upon the addition of cholesterol of up to 40%. Assuming that the membrane thickness does not change significantly (the thickness of the fully saturated membranes like DMPC was observed to increase only by about 15% in this range of cholesterol concentration[21]), the trend in the behaviour of K_a for membranes in the liquid ordered phase should be exhibited also by κ, namely the bending stiffness should increase significantly. This is not what is observed for the SM : Chol membranes. We can only conclude that the effect of cholesterol on K_a for DPPC membranes differs from that of SM bilayers, or that eqn (13) does not apply.

The bending stiffness of LE membranes was found to attain an intermediate value between that of DOPC : Chol and SM : Chol 1 : 1 membranes, see Fig. 4 and Table 1. We studied the influence of transmembrane peptides in the natural mixture on the bending stiffness of LE membranes. According to recent studies,[65,66] the protein area occupancy in the membrane core of synaptic vesicles and red blood cells is about 20%. Speculations about the influence of these protein domains on the fluidity of the membrane lead to the conclusion that plasma membranes may be more rigid and less fluid than it has been thought for several decades.[65] In addition, it has been suggested that studies of pure lipid bilayers do not fully reveal the properties of lipids in natural membranes. Contrary to this speculation, active proteins reconstituted in GUV were demonstrated to reduce the bending stiffness of the membranes.[67] Here, we employed vesicles made of LE membranes containing a naturally occurring variety of protein transmembrane domains. The results on the bending stiffness of such vesicles, as shown in Table 1, suggest that the presence of these transmembrane peptides has no appreciable effect on the membrane flexibility, contrary to the hypothesis proposed by Dupuy and Engelman.[65] Furthermore, previous measurements on whole red blood cells show even lower values for their bending stiffness (in the range 3–7 $\times$ 10^{-20} J)[68,69] arguing against this hypothesis. A recent report on the phase state of giant plasma membrane vesicles showed that the membrane is close to a critical point.[70] In such a state, the membrane properties may vary drastically, which may be the reason why the effect of transmembrane peptides on the membrane bending rigidity is not appreciable. To clarify this aspect, more data and evidence need to be collected.

Conclusions

The results reported here demonstrate that the mechanical properties of lipid membranes are governed primarily by the state of the lipid components. Cholesterol acts to modify the acyl chain order and probably also the interfacial membrane region and in this way influences the membrane mechanical properties. Our data suggest that the effect of cholesterol is not universal, but rather specific to the type of lipid. The bending rigidity of saturated or mono-unsaturated lipids like DMPC or POPC increases with cholesterol content, while that of double-unsaturated lipids like DOPC is independent of the cholesterol fraction. In sphingomyelin membranes the bending rigidity is found to decrease with increasing cholesterol content. We cannot argue that this behaviour is universal for the specific degree of unsaturation. A more plausible view would be that the effect of cholesterol depends on the individual molecular architecture of the lipid combining the effect of unsaturation and acyl chain length, and probably the lipid interfacial region. The results confirm that a generalization about the effect of cholesterol on

the bending rigidity is not possible. This emphasizes the need to further develop the methods for measuring the membrane flexibility in experimentally less demanding ways. The growing research activity on more complex membrane compositions accentuates this need even further. Here we reported two such methods which are fast and easy to use. The total measuring time is less than 20 min. Furthermore, these two approaches can be applied using widely available experimental equipment. In particular, the electrodeformation method can be reproduced using a simple homemade chamber with two electrodes and a microscope. The fluctuation analysis method needs a camera with a fast-speed shutter allowing exposure time shorter than 200 μs. Such cameras are now cheap and available on the market from various producers. Note that here we used an expensive and sophisticated fast-speed camera because it was available in the lab. Currently we perform the fluctuation analysis measurements on a conventional camera with a fast shutter. The approach based on fluctuation analysis can be applied both to neutral and charged membranes. The method based on vesicle electrodeformation has to be further adjusted in order to be applicable to salt solutions and charged membranes. Work in this direction is in progress.

Acknowledgements

We acknowledge S. Aranda, P. Vlahovska and P. Shchelokovskyy for useful discussions.

Notes and references

1 R. Dimova, S. Aranda, N. Bezlyepkina, V. Nikolov, K. A. Riske and R. Lipowsky, *J. Phys.: Condens. Matter*, 2006, **18**, S1151–S1176.
2 K. Simons and E. Ikonen, *Nature*, 1997, **387**, 569–572.
3 R. Lipowsky and R. Dimova, *J. Phys.: Condens. Matter*, 2003, **15**, S31–S45.
4 R. Lipowsky, *Nature*, 1991, **349**, 475–481.
5 R. Dimova, B. Pouligny and C. Dietrich, *Biophys. J.*, 2000, **79**, 340–356.
6 D. Marsh, *Chem. Phys. Lipids*, 2006, **144**, 146–159.
7 F. Brochard and J. F. Lennon, *J. Phys.*, 1975, **36**, 1035–1047.
8 R. M. Servuss, W. Harbich and W. Helfrich, *Biochim. Biophys. Acta, Biomembr.*, 1976, **436**, 900–903.
9 M. B. Schneider, J. T. Jenkins and W. W. Webb, *J. Phys.*, 1984, **45**, 1457–1472.
10 H. Engelhardt, H. P. Duwe and E. Sackmann, *J. Phys., Lett.*, 1985, **46**, 395–L400.
11 I. Bivas, P. Hanusse, P. Bothorel, J. Lalanne and O. Aguerrechariol, *J. Phys.*, 1987, **48**, 855–867.
12 J. F. Faucon, M. D. Mitov, P. Meleard, I. Bivas and P. Bothorel, *J. Phys.*, 1989, **50**, 2389–2414.
13 H. P. Duwe, J. Kaes and E. Sackmann, *J. Phys.*, 1990, **51**, 945–962.
14 J. R. Henriksen and J. H. Ipsen, *Eur. Phys. J. E*, 2002, **9**, 365–374.
15 M. Kummrow and W. Helfrich, *Phys. Rev. A: At., Mol., Opt. Phys.*, 1991, **44**, 8356–8360.
16 G. Niggemann, M. Kummrow and W. Helfrich, *J. Phys. II*, 1995, **5**, 413–425.
17 J. B. Manneville, P. Bassereau, D. Levy and J. Prost, *Phys. Rev. Lett.*, 1999, **82**, 4356–4359.
18 M. D. E. Faris, D. Lacoste, J. Pecreaux, J. F. Joanny, J. Prost and P. Bassereau, *Phys. Rev. Lett.*, 2009, **102**, 038102.
19 N. Gov, A. G. Zilman and S. Safran, *Phys. Rev. Lett.*, 2003, **90**, 228101.
20 J. Pan, S. Tristram-Nagle, N. Kucerka and J. F. Nagle, *Biophys. J.*, 2008, **94**, 117–124.
21 J. J. Pan, T. T. Mills, S. Tristram-Nagle and J. F. Nagle, *Phys. Rev. Lett.*, 2008, **100**, 198103.
22 E. G. Bligh and W. J. Dyer, *Can. J. Biochem. Physiol.*, 1959, **37**, 911–917.
23 K. A. Riske, R. L. Knorr and R. Dimova, *Soft Matter*, 2009, **5**, 1983–1986.
24 T. Nakano, Y. Wada and S. Matsumura, *Clin. Hemorheol. Microcirc.*, 2001, **24**, 85–92.
25 M. I. Angelova and D. S. Dimitrov, *Faraday Discuss. Chem. Soc.*, 1986, **81**, 303–311.
26 J. Pecreaux, H. G. Dobereiner, J. Prost, J. F. Joanny and P. Bassereau, *Eur. Phys. J. E*, 2004, **13**, 277–290.
27 A. Tian and T. Baumgart, *Biophys. J.*, 2009, **96**, 2676–2688.
28 B. Sorre, A. Callan-Jones, J. B. Manneville, P. Nassoy, J. F. Joanny, J. Prost, B. Goud and P. Bassereau, *Proc. Natl. Acad. Sci. U. S. A.*, 2009, **106**, 5622–5626.
29 T. R. Weikl and R. Lipowsky, *Phys. Rev. E: Stat., Nonlinear, Soft Matter Phys.*, 2001, **64**, 011903.
30 V. D. Gordon, M. Deserno, C. M. J. Andrew, S. U. Egelhaaf and W. C. K. Poon, *Europhys. Lett.*, 2008, **84**, 48003.
31 S. T. Milner and S. A. Safran, *Phys. Rev. A: At., Mol., Opt. Phys.*, 1987, **36**, 4371–4379.
32 W. Hackl, U. Seifert and E. Sackmann, *J. Phys. II*, 1997, **7**, 1141–1157.
33 U. Seifert, *Z. Phys. B: Condens. Matter*, 1995, **97**, 299–309.
34 J. Solon, J. Pecreaux, P. Girard, M. C. Faure, J. Prost and P. Bassereau, *Phys. Rev. Lett.*, 2006, **97**, 098103.
35 W. Harbich and W. Helfrich, *Z. Naturforsch., A: Phys. Sci.*, 1979, **34**, 1063–1065.
36 R. Dimova, K. A. Riske, S. Aranda, N. Bezlyepkina, R. L. Knorr and R. Lipowsky, *Soft Matter*, 2007, **3**, 817–827.
37 S. Aranda, K. A. Riske, R. Lipowsky and R. Dimova, *Biophys. J.*, 2008, **95**, L19–L21.
38 R. Dimova, N. Bezlyepkina, M. D. Jordö, R. L. Knorr, K. A. Riske, M. Staykova, P. M. Vlahovska, T. Yamamoto, P. Yang and R. Lipowsky, *Soft Matter*, 2009, **5**, 3201–3212.
39 W. Helfrich and R. M. Servuss, *Nuovo Cimento Soc. Ital. Fis., D*, 1984, **3**, 137–151.
40 E. Evans and W. Rawicz, *Phys. Rev. Lett.*, 1990, **64**, 2094–2097.
41 P. M. Vlahovska, R. S. Gracia, S. Aranda-Espinoza and R. Dimova, *Biophys. J.*, 2009, **96**, 4789–4803.
42 S. L. Veatch and S. L. Keller, *Phys. Rev. Lett.*, 2005, **94**, 148101.
43 S. Semrau, T. Idema, L. Holtzer, T. Schmidt and C. Storm, *Phys. Rev. Lett.*, 2008, **100**, 088101.
44 J. R. Henriksen and J. H. Ipsen, *Eur. Phys. J. E*, 2004, **14**, 149–167.
45 W. Rawicz, K. C. Olbrich, T. McIntosh, D. Needham and E. Evans, *Biophys. J.*, 2000, **79**, 328–339.
46 M. Staykova, R. Lipowsky and R. Dimova, *Soft Matter*, 2008, **4**, 2168–2171.
47 E. Evans and D. Needham, *J. Phys. Chem.*, 1987, **91**, 4219–4228.
48 J. B. Song and R. E. Waugh, *Biophys. J.*, 1993, **64**, 1967–1970.
49 A. Roux, D. Cuvelier, P. Nassoy, J. Prost, P. Bassereau and B. Goud, *EMBO J.*, 2005, **24**, 1537–1545.
50 J. C. Mathai, S. Tristram-Nagle, J. F. Nagle and M. L. Zeidel, *J. Gen. Physiol.*, 2007, **131**, 69–76.
51 P. Meleard, C. Gerbeaud, T. Pott, L. FernandezPuente, I. Bivas, M. D. Mitov, J. Dufourcq and P. Bothorel, *Biophys. J.*, 1997, **72**, 2616–2629.
52 J. Henriksen, A. C. Rowat, E. Brief, Y. W. Hsueh, J. L. Thewalt, M. J. Zuckermann and J. H. Ipsen, *Biophys. J.*, 2006, **90**, 1639–1649.
53 T. P. W. McMullen, R. N. A. H. Lewis and R. N. McElhaney, *Curr. Opin. Colloid Interface Sci.*, 2004, **8**, 459–468.
54 A. Filippov, G. Oradd and G. Lindblom, *Biophys. J.*, 2006, **90**, 2086–2092.
55 R. F. M. de Almeida, A. Fedorov and M. Prieto, *Biophys. J.*, 2003, **85**, 2406–2416.
56 M. I. Collado, F. M. Goni, A. Alonso and D. Marsh, *Biochemistry*, 2005, **44**, 4911–4918.
57 P. J. Quinn and C. Wolf, *Biochim. Biophys. Acta, Biomembr.*, 2009, **1788**, 1877–1889.
58 F. M. Goni, A. Alonso, L. A. Bagatolli, R. E. Brown, D. Marsh, M. Prieto and J. L. Thewalt, *Biochim. Biophys. Acta, Mol. Cell Biol. Lipids*, 2008, **1781**, 665–684.
59 D. A. Mannock, T. J. McIntosh, X. Jiang, D. F. Covey and R. N. McElhaney, *Biophys. J.*, 2003, **84**, 1038–1046.
60 A. Tsamaloukas, H. Szadkowska and H. Heerklotz, *Biophys. J.*, 2006, **90**, 4479–4487.

61 R. Goetz, G. Gompper and R. Lipowsky, *Phys. Rev. Lett.*, 1999, **82**, 221–224.
62 D. Boal, *Mechanics of the Cell*, Cambridge University Press, Cambridge, 2002.
63 W. Rawicz, B. A. Smith, T. J. Mclntosh, S. A. Simon and E. Evans, *Biophys. J.*, 2008, **94**, 4725–4736.
64 K. J. Tierney, D. E. Block and M. L. Longo, *Biophys. J.*, 2005, **89**, 2481–2493.
65 A. D. Dupuy and D. M. Engelman, *Proc. Natl. Acad. Sci. U. S. A.*, 2008, **105**, 2848–2852.
66 S. Takamori, M. Holt, K. Stenius, E. A. Lemke, M. Gronborg, D. Riedel, H. Urlaub, S. Schenck, B. Brugger, P. Ringler, S. A. Muller, B. Rammner, F. Grater, J. S. Hub, B. L. De Groot, G. Mieskes, Y. Moriyama, J. Klingauf, H. Grubmuller, J. Heuser, F. Wieland and R. Jahn, *Cell*, 2006, **127**, 831–846.
67 P. Girard, J. Prost and P. Bassereau, *Phys. Rev. Lett.*, 2005, **94**, 088102.
68 A. Zilker, H. Engelhardt and E. Sackmann, *J. Phys.*, 1987, **48**, 2139–2151.
69 G. Popescu, T. Ikeda, K. Goda, C. A. Best-Popescu, M. Laposata, S. Manley, R. R. Dasari, K. Badizadegan and M. S. Feld, *Phys. Rev. Lett.*, 2006, **97**, 218101.
70 S. L. Veatch, P. Cicuta, P. Sengupta, A. Honerkamp-Smith, D. Holowka and B. Baird, *ACS Chem. Biol.*, 2008, **3**, 287–293.

Effect of cholesterol on the rigidity of saturated and unsaturated membranes: fluctuation and electrodeformation analysis of giant vesicles

Rubèn Serral Gracià, Natalya Bezlyepkina, Roland L. Knorr, Reinhard Lipowsky and Rumiana Dimova*

Max Planck Institute of Colloids and Interfaces, Science Park Golm, 14424 Potsdam, Germany

Supplementary Information

1. Proteoliposome preparation and lipid extraction from red blood cells

Fresh human red blood cells (RBC) (courtesy of Nina Geldmacher from the Max Planck Institute for Infection Biology, Berlin) were purified according to the method described in detail in [1]. The RBC were washed 4 times in cold isotonic buffer (145 mM NaCl, 5 mM KCl, 5 mM Hepes, pH 7.4 at 4 °C) and centrifuged 10 min at 2000 × *g* at 4 °C. Then, the cells were lysed by shaking 10 min on ice in hypotonic solution (15 mM KCl, 0.01 mM EDTA, 1 mM EGTA, 5 mM Hepes, pH 6.0). EDTA, EGTA and Hepes were purchased from Sigma-Aldrich, Germany. The ghosts were washed once in hypotonic solution without EGTA and twice in hypotonic solution without EGTA but with 2 mM Mg^{2+} and centrifuged for 10 min at 4°C and 12000 × *g*. To remove peripherally associated proteins (and remaining hemoglobin, which is known to contaminate lipid extracts [2]) from the membrane of the open RBC ghosts, they were shaken for 30 min on ice in 10 mM NaOH and centrifuged. The membranes were subjected to protein digestion with proteinase K (final concentration of 3 mg/ml, over night at room temperature), which reduces remaining proteins within the bilayer to their transmembrane helices [1]. Digestion was stopped by adding Pefabloc (5 mM final concentration) and incubation for 30 min. Five washing steps removed all remaining proteinase K and its inhibitor. The last wash was done with 10 mM glucose. Proteoliposomes were dried on conductive glasses and used for vesicles formation as described in the main text. Proteoliposomes contain about 20 area % transmembrane proteins [1].

For preparation of lipid extracts not containing transmembrane peptides, the lipids were extracted from the proteoliposomes using the method of Bligh and Dyer [3]. Briefly, the centrifuged pellet was diluted with bidistilled water to a volume of 1.2 ml, followed by stepwise addition and vortexing of the following solutions: 1.5 ml chloroform, 3 ml methanol, 1.5 ml chloroform, 1.5 ml bidistilled water. After 5 min centrifugation of the obtained solution at 2000 × *g*, the chloroform-rich phase was separated, stored at -80°C and used for vesicle preparation.

2. Contour recognition

We used a home-developed program for recognizing the vesicle contour from the acquired images. The program uses libtiff [4] to read the images and Qt4 [5] to display and treat them. The rest is done in C/C++ and compiled with GNU tools for either Linux or Windows using mingw [6] and DevCpp [7]. For the mathematical treatment Numerical Recipes in C was used [8]. The program reads the images, between 2000 and 8000, and displays them. The contour finding algorithm is split in two parts, first the contour is grossly found, i.e. with pixel resolution, and then it is refined by fitting intensity decays, achieving a resolution better than one pixel.

The first part closely follows the approach in [9]. Initially, the search of the contour is restricted to a circular shell (or an elongated circle, a stadium shape), defined by two concentric circles with different radius. The user chooses these radii considering that the contour of the vesicle in all images is contained within the shell. The intensity profiles in the radial direction for *N* different angles in this shell are extracted from the image by linear interpolation of the pixel value. Gaussian interpolation was also used, but it did not lead to better results while considerably decreasing the speed of the algorithm. For regions of interest with a stadium shape, i.e. in the case of prolate vesicles, two linear and two angular parts were taken. The extracted intensity values from the angular sections define a rectangular trellis from the unwrapping of the shell. Figure S1 schematically illustrates this process.

At this stage, the vesicle contour is represented by an approximately dark line going through the middle of the rectangular trellis, as shown in the last cartoon in Fig. S1. Thus, finding the contour reduces to locating the path joining the two sides of the rectangle with a minimal given cost. In the following, we explain the algorithm used for this purpose.

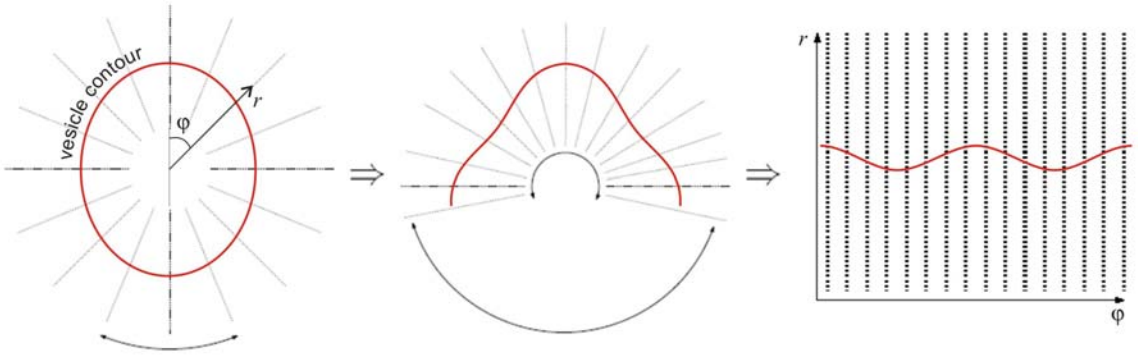

Figure S1. Unwrapping of the trellis to construct a rectangular system for the detection of the vesicle contour. In the first sketch, the contour of an elliptical vesicle is schematically represented by the red curve.

Two scenarios were considered. Both of them have in common that first the gross location of the vesicle contour is found (see next section for a detailed description). After that, we fit the gray value intensity profile around the points from the contour in order to determine it with sub-pixel resolution. The first scenario consists of finding the path with minimal/maximal transversal derivative. Note that a transversal derivative in the trellis corresponds to a radial derivative in the real image (see Fig. S1). Using this approach the steepest part of the intensity profile is found (see Fig. S2).This approach has been previously used in [10], where vesicles filled with sucrose and immersed in glucose were used. The two solutions have different refractive index making the vesicle body look darker than the background. Thus, the intensity profile of a line crossing the contour has a sigmoidal shape. The procedure finds the steepest descending/ascending zone in the line profile and fits it with a straight line. The cross point of this line with the mean gray level of the image give the position of the vesicle contour. The deficiency of this procedure is that perfectly homogeneous illumination is required and no defects (points of significantly different intensity due to, for example, dirt in the sample or in the optics) should be present near the vesicle contour. These problems are overcome in the second scenario, which was primarily used in this work. The contour position is defined as the minimum of the valley in the intensity profile of a line crossing the vesicle contour; see Fig. S2 for one example from a vesicle with no glucose/sucrose contrast enhancement. Note that for vesicles with glucose/sucrose asymmetry, the intensity line profile is not symmetric like in Fig. S2 but has a sigmoidal shape (to illustrate the first approach, we consider a half of the profile, as indicated in the figure). We find the minimum of the intensity profile in gross. Then the two sides of the valley around the minimum are fitted using straight lines and the crossing point defines the location of the vesicle surface; see Fig. S2. The error of this intersection is found from the errors in the fit parameters. In some cases, the fit can be very inaccurate due to defects in the image or impurities. If the location of the intersection (determined with sub-pixel resolution) differs more than 3 pixels from the grossly determined minimum in the line profile, the latter is taken and an error bar of ±1 pixel is given.

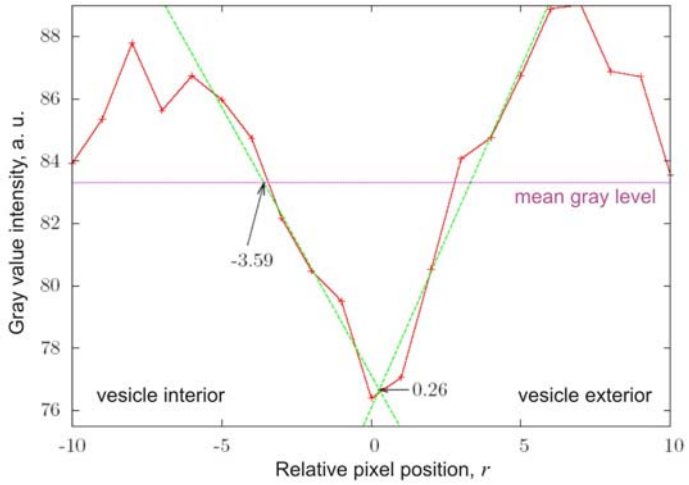

Figure S2. Typical intensity profile of a line crossing the vesicle contour in a phase contrast microscopy image of a vesicle filled with and immersed in the same solution. From the pixel intensity one can locate the valley of the profile (here for convenience placed at $y = 0$) yielding the contour position with pixel resolution. The horizontal line indicates the mean gray level. According to the first protocol, the contour is located at $y = -3.59$ (we have considered only the left half of the intensity profile). The intersection of the steep line in the profile and the horizontal line is used to define the position of the vesicle contour. According to the second protocol (predominantly used in this work), the vesicle contour is located by fitting the two slopes around the minimum with straight lines (green dashed lines). Their intersection provides a definition of the minimum of the valley, i.e., the location of the vesicle contour in sub-pixel resolution, $y = 0.26$.

Finding the gross contour of a vesicle: In order to find the gross position of the contour we used an efficient dynamical programming algorithm, the so-called Viterbi algorithm. This algorithm uses the fact that if the path with minimal cost from A to C crosses B, the path B to C is also minimal. The algorithm we used is as follows. We consider a trellis with length l and width w. Every point of the trellis is given a weight, I, for instance the value of the derivative in a given direction (the first scenario described above) or the gray value intensity (second scenario). To find the minimum path, a weight function is defined as

$$F_{i,v} = I_{i,v} + \min (F_{i-1,v-1}, F_{i-1,v}, F_{i-1,v+1}) \quad \text{(S1)}$$

where v varies from 1 to w and i varies from 1 to l, and min denotes the minimum value. To fill up the matrix F, one starts from one end of the trellis $i = 1$ (whereby $F_{0,v} = 0$), and evolves step by step till the other end $i = w$. Note that the values of a column $i - 1$ define the values at column i. Once the end of trellis is reached, the minimum $F_{l,v}$ is taken and the minimal path is found by retracing back the choices made for the minimum in eq. (S1). Since we look for a continuous path, without jumps, in the weight definition eq. (S1) we restrict the search to the nearest neighbors only, $v - 1$, $v + 1$. Other options like penalizing curvature have been proposed in literature [9].

This procedure does not necessarily yield a closed vesicle contour, i.e. the last point does not necessarily coincide with the first one. To solve this problem we make use of periodic boundary conditions. The trellis is extended with several points (typically 10 or more), i.e. the beginning of the trellis is copied in the end of it proceeding with the algorithm in eq. (S1). The initial, repeated points, are neglected afterwards, when retracing the path. This procedure proved very successful in closing the contour in about all our images.

The error of the contour is defined as the maximal error of all the points. If this error exceeds a certain threshold, the contour is rejected from the analysis. Furthermore, the contour must be a continuous line; therefore neighboring points must have approximately the same radius. Thus, contours showing large jumps are rejected as well.

Once the contour is found, its center of mass is used to center a shell (two concentric circles) confining the vesicle contour, which is used as a starting search area for the next image. This procedure properly follows the movements of the vesicle if they are not too abrupt and the shell width is large enough. Even vesicles which partially move out of the image borders and come back are followed successfully (the incomplete contours are of course neglected).

3. Dye exclusion from solid domains in vesicles in the three-phase coexistence range

We prepared vesicles composed of DOPC, egg SM and cholesterol with 40:40:20 molar ratio following the method described in the main text. Membranes with this composition at low temperatures like 10°C lie in the region of coexistence of solid (S), liquid ordered (Lo) and liquid disordered (Ld) phases. Thus the vesicles exhibit three types of domains. The membranes also contained small fractions of two dyes (0.3 mol %): perylene and diIC18. diIC18 preferentially partitions in the Ld phase and is excluded from the other domains. Perylene partitions in the Lo and in the Ld phases and is also excluded from the S domains. When observed with confocal microscopy, as shown in Fig. S3, vesicles with three-phase coexistence exhibit Ld domains (red), Lo domains (green) and S domains (black); see Fig. S3. Note that the Ld and Lo domains have smooth boundaries when they are in contact with each other, and rough borders when in contact with the S domains. In two-phase SM:Chol vesicles containing Lo and S domains, perylene should be also excluded from the S domains, and thus can be used as an indicator for their presence. Since we did not observe such exclusion in these vesicles, we conclude that the membranes were either in the liquid ordered state, or that the solid domains were smaller than 1 μm.

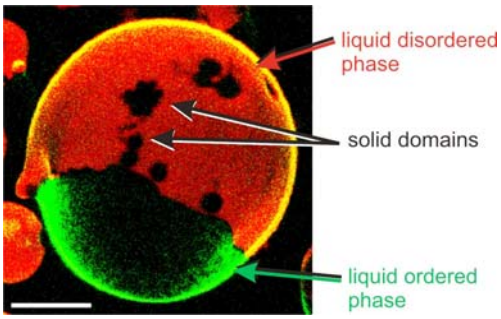

Figure S3. Three phase coexistence in a vesicle composed of DOPC:SM:Chol 40:40:20 at 8.5°C. The scale bar corresponds to 20 μm.

References:

1 A. D. Dupuy and D. M. Engelman, *Proc. Natl. Acad. Sci. USA*, 2008, **105**, 2848-2852.
2 H. G. Rose and M. Oklander, *J. Lipid Res.*, 1965, **6**, 428-431.
3 E. G. Bligh and W. J. Dyer, *Can. J. Biochem. Physiol.*, 1959, **37**, 911-917.
4 http://www.libtiff.org
5 http://trolltech.com/
6 http://www.mingw.org/
7 http://www.bloodshed.net/
8 W. T. Vetterling, W. H. Press, S. A. Teukolsky, and B. P. Flannery, Numerical Recipes in C, Cambridge University Press, 2nd ed., 1997.
9 P. Bamford and B. Lovell, *Signal Processing*, 1998, **71**, 203-213.
10 J. Pecreaux, H. G. Dobereiner, J. Prost, J. F. Joanny and P. Bassereau, *Eur. Phys. J. E*, 2004, **13**, 277-290.